

A Generalized Stationary Algorithm for Resonant Tunneling: Multi-Mode Approximation and High Dimension

Naoufel Ben Abdallah[†] and Hao Wu^{1,2,*}

¹ *Department of Mathematical Sciences, Tsinghua University, Beijing, 10084, China.*

² *Institut de Mathématiques de Toulouse, Université Paul Sabatier, 118, route de Narbonne, 31062 Toulouse Cedex, France.*

Received 4 June 2010; Accepted (in revised version) 13 October 2010

Available online 13 June 2011

Abstract. The multi-mode approximation is presented to compute the interior wave function of Schrödinger equation. This idea is necessary to handle the multi-barrier and high dimensional resonant tunneling problems where multiple eigenvalues are considered. The accuracy and efficiency of this algorithm is demonstrated via several numerical examples.

AMS subject classifications: 35C99, 65N99, 81Q05

Key words: Schrödinger equation, numerical scheme, resonant tunneling, multi-mode approximation, high dimension.

1 Introduction

The resonant tunneling diode (RTD) is a diode with a resonant tunneling structure in which electrons can tunnel through some resonant states at certain energy levels. It has been widely studied both theoretically and experimentally [7, 8, 10] for its important role in constituting different functions of the nanoscale semiconductor devices, e.g. integrated circuit, microprocessor, memory devices, wide-band wired and wireless communications [21, 27]. The RTD is made up of two large reservoirs and an active region. The reservoirs, which are highly conducting, can be used for exchanging electrons with external electrical circuit. The active region (see Fig. 1) can be a double barrier, triple barrier, quantum well, quantum wire, quantum dot, etc.

[†]It is so sad that the author has passed away.

*Corresponding author. *Email address:* hwu@tsinghua.edu.cn (H. Wu)

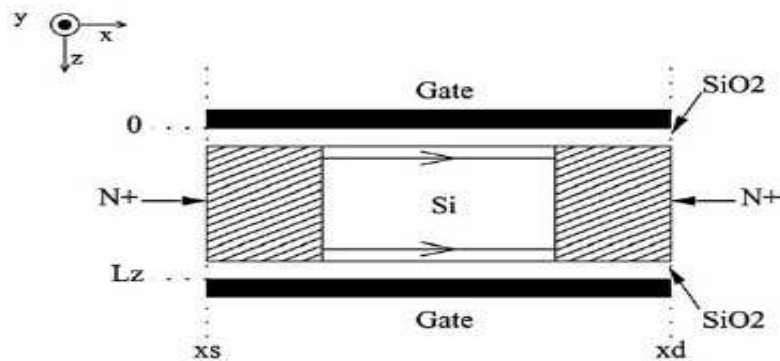


Figure 1: The picture of two dimensional device for the active region of RTD. This figure is copied from [24].

Since the length scale is small in RTD, quantum effects should be considered. Therefore a general approach to model such device is through the Schrödinger equation for wave function coupled to Poisson equation for the electric potential [20].

There are two primary issues in the numerical simulation. One is the numerical integration of the Schrödinger equation, e.g. finite difference method [18, 19], spectral type method [5, 6, 22], the WKB-scheme [3, 4], and the Gaussian beam method [14, 15]. The other is the reduction of energy grid points [4, 9, 23]. Besides these, the artificial boundary conditions [1, 2, 17], the dimensionality reduction [3, 24], the Gummel iteration [11, 23], the Green function's method [12, 13, 26] and many other related topics are investigated.

The well known numerical difficult in RTD is that the curve of transmission coefficient versus energy tends to be singular in the vicinity of resonant energies. Therefore, a very fine energy mesh is needed to capture the correct integral of the density, which results a large supplementary numerical cost for computing these Schrödinger equations. In order to deal with this problem, an adaptive energy mesh method was developed in [23]. But it still consume lots of computational resource since the mesh should be very fine near the resonant energies. Moreover, it doesn't work for the time dependent case because the resonances move.

Lately, the one mode approximation [4, 16, 25] was proposed to compute the density. The method decompose the wave function into an exterior part and an interior part. The exterior part is smooth in energy mesh and thus does not require a fine energy mesh. The interior part can be well approximated by its projection on the resonant state. The one-mode approximation does save the computational cost, but this approximation may not work for some applications, e.g. multiple barrier problem and high dimensional problem.

In this paper, we present the multi-mode approximation to overcome these difficulties. The one dimensional problem is discussed in Section 2. In Section 3, it is extended for high dimensions. We conduct numerical examples in Section 4 to verify the accuracy of the numerical methods. In Section 5, we give some discussions on the algorithm efficiency. Finally, we make the conclusive remarks in Section 6.

2 The one dimensional stationary algorithm

Consider the dimensionless Schrödinger equation with open boundary condition on the domain $[a, b]$

$$\begin{cases} -\frac{1}{2}\epsilon^2 \varphi_p'' + V \varphi_p = E_p^a \varphi_p, & (p \geq 0), \\ \epsilon \varphi_p'(a) + ip \varphi_p(a) = 2ip, \\ \epsilon \varphi_p'(b) - i\sqrt{p^2 + 2(V(a) - V(b))} \varphi_p(b) = 0, \end{cases} \quad (2.1)$$

for electrons injected at $x = a$ with momentum $p \geq 0$ and

$$\begin{cases} -\frac{1}{2}\epsilon^2 \varphi_p'' + V \varphi_p = E_p^b \varphi_p, & (p \leq 0), \\ \epsilon \varphi_p'(b) + ip \varphi_p(b) = 2ip, \\ \epsilon \varphi_p'(a) - i\sqrt{p^2 + 2(V(b) - V(a))} \varphi_p(a) = 0, \end{cases} \quad (2.2)$$

for electrons injected at $x = b$ with momentum $p \leq 0$. Here

$$E_p^a = \frac{1}{2}p^2 + V(a), \quad E_p^b = \frac{1}{2}p^2 + V(b),$$

$\varphi_p(x)$ is the wave function, ϵ is the re-scaled Planck constant, and the electrostatic potential V is split into the external potential V_e and the self-consistent potential V_s :

$$V(x) = V_e(x) + V_s(x).$$

The self-consistent potential V_s satisfies the Poisson equation

$$\begin{cases} V_s''(x) = -\frac{1}{\epsilon_0} (n(x) - n_D(x)), \\ V_s(a) = V_s(b) = 0, \end{cases} \quad (2.3)$$

in which ϵ_0 is the dielectric constant, n_D is the doping density, and the electronic density $n(x)$ is given by

$$n(x) = \int_{-\infty}^{+\infty} g(p) |\varphi_p(x)|^2 dp. \quad (2.4)$$

In the integral, $g(p)$ is the statistics of the electrons injected at $x = a$ or $x = b$, e.g. the Fermi-Dirac statistic. The external potential (Fig. 2)

$$V_e(x) = V_b(x) + V_w(x) + V_a(x),$$

is a summation of quantum barrier, quantum well

$$V_b(x) = V_0 1_{[a_2, b_2]}, \quad V_w(x) = -V_0 1_{[c_1, d_1] \cup [c_2, d_2] \cup \dots \cup [c_F, d_F]},$$

and the applied bias

$$V_a(x) = -V_1 \left(\frac{x - a_1}{b_1 - a_1} 1_{[a_1, b_1]} + 1_{[b_1, b]} \right).$$

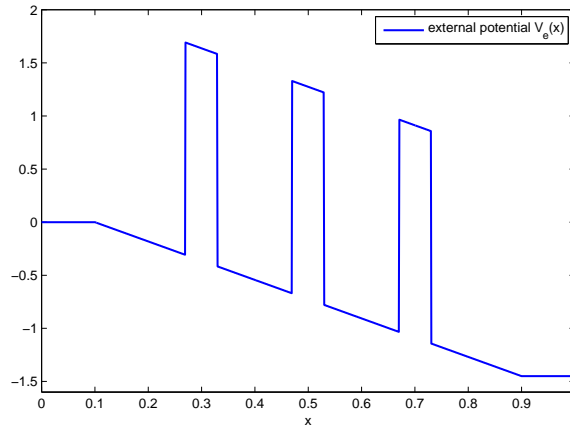


Figure 2: The external potential $V_e(x)$.

Here $V_0 \geq 0$ and $V_1 \geq 0$ denotes the height of the barrier and the amplitude of the applied bias respectively. And we have

$$a < a_1 < a_2 < c_1 < d_1 < \dots < c_F < d_F < b_2 < b_1 < b.$$

To solve the stationary Schrödinger-Poisson equations (2.1)-(2.4) iteratively, there are mainly three steps:

1. Compute the wave function $\varphi_{p_k}^l(x)$ from $V_s^l(x)$ with different momentum p_k by solving the Schrödinger equation (2.1)-(2.2).
2. Numerical integrate the quantity $g(p_k) \left| \varphi_{p_k}^l(x) \right|^2$ into the density $n^l(x)$ with the integration formula (2.4).
3. Compute the self-consistent potential at next iteration $V_s^{l+1}(x)$ from $n^l(x)$ by solving the poisson equation (2.3).

Here l denotes the times of iteration and $\{p_k\}$ gives the energy mesh discretization. In this paper, we focus on improving the first step, which is to implement the multi-mode approximation into the numerical schemes for (2.1)-(2.2). For the second and the third step, we refer readers to the adaptive mesh approach for the integration [4, 23] and the Gummel iteration for the coupling [11, 23].

2.1 Multi-mode approximations

To concentrate on the multi-mode approximation for the Schrödinger equation, we ignore the effect of the self-consistent potential $V_s(x) = 0$, and only inject electrons at $x = a$ with momentum $p \geq 0$. Then we rewrite the equation (2.1) as

$$\begin{cases} -\frac{1}{2}\epsilon^2 \varphi_p'' + V_e \varphi_p = \frac{1}{2} p^2 \varphi_p, \\ \epsilon \varphi_p'(a) + i p \varphi_p(a) = 2 i p, \\ \epsilon \varphi_p'(b) - i \sqrt{p^2 + 2V_1} \varphi_p(b) = 0. \end{cases} \quad (2.5)$$

The transmission coefficients versus energy is defined by

$$T(E) = \sqrt{\frac{E+V_1}{E}} |\varphi_p(b)|^2,$$

with $E = \frac{1}{2}p^2$. Following the previous paper [4,9,16,25], we decompose the wave function φ_p into an exterior part φ_p^{ext} and an interior part φ_p^{int} ,

$$\varphi_p(x) = \varphi_p^{ext}(x) + \varphi_p^{int}(x).$$

The exterior wave function is defined as the solution of

$$\begin{cases} -\frac{1}{2}\epsilon^2 \partial_{xx} \varphi_p^{ext} + (V_b + V_a) \varphi_p^{ext} = \frac{1}{2}p^2 \varphi_p^{ext}, \\ \epsilon \partial_x \varphi_p^{ext}(a) + ip \varphi_p^{ext}(a) = 2ip, \\ \epsilon \partial_x \varphi_p^{ext}(b) - i\sqrt{p^2 + 2V_1} \varphi_p^{ext}(b) = 0. \end{cases} \quad (2.6)$$

Since φ_p^{ext} is smooth on the energy direction p , it can be computed initially on a coarse mesh of p and then interpolated for finer requirements [4]. Then the interior wave function satisfies the nonhomogeneous Schrödinger equation

$$\begin{cases} -\frac{1}{2}\epsilon^2 \partial_{xx} \varphi_p^{int} + V_e \varphi_p^{int} = \frac{1}{2}p^2 \varphi_p^{int} - V_w \varphi_p^{ext}, \\ \epsilon \partial_x \varphi_p^{int}(a) + ip \varphi_p^{int}(a) = 0, \\ \epsilon \partial_x \varphi_p^{int}(b) - i\sqrt{p^2 + 2V_1} \varphi_p^{int}(b) = 0. \end{cases} \quad (2.7)$$

The direct simulation of (2.7) is waste of computational resource. Instead, we approximate it by the multi-mode form

$$\varphi_p^{int}(x) = \sum_{n=1}^N \frac{\theta_n(p)}{\lambda_n - \frac{1}{2}p^2} \phi_n(x). \quad (2.8)$$

Here $\phi_n(x)$ is the non trivial solution of the eigenvalue problem

$$\begin{cases} -\frac{1}{2}\epsilon^2 \partial_{xx} \phi + V_e \phi = \lambda \phi, \\ \epsilon \partial_x \phi(a) + i\sqrt{2\lambda} \phi(a) = 0, \\ \epsilon \partial_x \phi(b) - i\sqrt{2(\lambda + V_1)} \phi(b) = 0, \end{cases} \quad (2.9)$$

here $\sqrt[3]{z}$ denotes the determination of the square root which is holomorphic on $\mathbb{C} \setminus i\mathbb{R}_-$ and defined as follows: for $z = \rho e^{i\theta}$, with $\rho > 0$ and $\theta \in (-\frac{\pi}{2}, \frac{3\pi}{2})$, $\sqrt[3]{z} = \sqrt{\rho} e^{i\frac{\theta}{2}}$. The complex eigenvalue $\lambda = E_R - i\Gamma/2$ has necessary a non vanishing imaginary part. Taking (2.8)-(2.9) into (2.7) leads to the linear system for the coefficients $\theta_n(p)$:

$$\sum_{n=1}^N \langle \phi_n, \phi_{n'} \rangle \theta_n(p) = -\langle V_w \varphi_p^{ext}, \phi_{n'} \rangle. \quad (2.10)$$

Here $\langle \cdot, \cdot \rangle$ denotes the inner product. Since Eq. (2.9) is nonlinear eigenvalue problem, the eigenfunctions are not orthogonal to the others. It is easy to see that the multi-mode approximation is consistent with the one mode approximation.

Remark 2.1. Note the boundary conditions are different in (2.7) and (2.9), but this is still a good approximation. The detailed explanation can be found in [4].

Remark 2.2. The numerical method of non trivial eigenvalue problem (2.9) can be found in [4, 9]. For this reason, we do not discuss here.

3 Generalization to higher dimensions

The idea of multi-mode approximation can be generalized to higher dimensions naturally. Here we take the 2d problem as an example to explain the necessary processes. The modeling approach used here can be as well extended to 3d problems. Consider the 2d Schrödinger equation

$$-\frac{1}{2}\epsilon^2 (\partial_{xx}\varphi_E + \partial_{yy}\varphi_E) + V_e(x,y)\varphi_E = E\varphi_E, \tag{3.1}$$

on computational domain $\Omega = [a,b] \times [-d,d]$. Let $\partial\Omega = \Gamma_d \cup \Gamma_a \cup \Gamma_b$ with

$$\begin{aligned} \Gamma_d &= \{(x,y) \mid x \in [a,b], y = \pm d\}, \\ \Gamma_a &= \{(a,y) \mid y \in [-d,d]\}, \\ \Gamma_b &= \{(b,y) \mid y \in [-d,d]\}. \end{aligned}$$

Then the boundary conditions are

$$\varphi_E(x,y)|_{\Gamma_d} = 0, \tag{3.2a}$$

$$\epsilon \partial_x \varphi_E(a,y) = \sum_{E > E_m^a} i \sqrt{2(E - E_m^a)} (2a_m - \varphi_{E,m}^a) \chi_m^a(y) + \sum_{E \leq E_m^a} \sqrt{2(E_m^a - E)} \varphi_{E,m}^a \chi_m^a(y), \tag{3.2b}$$

$$\epsilon \partial_x \varphi_E(b,y) = \sum_{E > E_m^b} i \sqrt{2(E - E_m^b)} \varphi_{E,m}^b \chi_m^b(y) - \sum_{E \leq E_m^b} \sqrt{2(E_m^b - E)} \varphi_{E,m}^b \chi_m^b(y). \tag{3.2c}$$

Here $(E_m^*, \chi_m^*(y))$ ($*$ = a, b) are solutions of the eigenvalue problem

$$\begin{cases} -\frac{1}{2}\epsilon^2 \partial_{yy} \chi^*(y) + V_e(*,y) \chi^*(y) = E^* \chi^*(y), \\ \chi^*(\pm d) = 0, \quad \langle \chi^*(y), \chi^*(y) \rangle = 1. \end{cases} \tag{3.3}$$

We also have

$$\begin{aligned} \varphi_E(a,y) &= \sum_{m=1}^{\infty} \varphi_{E,m}^a \chi_m^a(y), & \text{where } \varphi_{E,m}^a &= \langle \varphi_E(a,y), \chi_m^a(y) \rangle, \\ \varphi_E(b,y) &= \sum_{m=1}^{\infty} \varphi_{E,m}^b \chi_m^b(y), & \text{where } \varphi_{E,m}^b &= \langle \varphi_E(b,y), \chi_m^b(y) \rangle. \end{aligned}$$

The coefficients of incoming waves a_m and the energy E are given here. The external potential

$$V_e(x,y) = V_b(x,y) + V_w(x,y) + V_a(x,y)$$

is also a summation of quantum barrier, quantum well

$$V_b(x,y) = V_0 \mathbf{1}_{\Omega_b}, \quad V_w(x,y) = -V_0 \mathbf{1}_{\Omega_1 \cup \Omega_2 \cup \dots \cup \Omega_F}$$

and the applied bias

$$V_a(x,y) = -\frac{x-a}{b-a} V_1(y).$$

Here $V_0 \geq 0$ and $V_1(y) \geq 0$ denotes the height of the barrier and the amplitude of the applied bias respectively. And we have

$$\Omega_f \subset \Omega_b \subset \Omega \quad (1 \leq f \leq F), \quad \Omega_f \cap \Omega_{f'} = \emptyset \quad (1 \leq f < f' \leq F).$$

Similarly with the one dimensional case, we decompose the wave function φ_E into an exterior part φ_E^{ext} and an interior part φ_E^{int} ,

$$\varphi_E(x,y) = \varphi_E^{ext}(x,y) + \varphi_E^{int}(x,y).$$

The exterior wave function is defined as the solution of

$$-\frac{1}{2}\epsilon^2 (\partial_{xx} \varphi_E^{ext} + \partial_{yy} \varphi_E^{ext}) + (V_b + V_a) \varphi_E^{ext} = E \varphi_E^{ext}, \tag{3.4}$$

with the same condition as (3.2). And the interior wave function satisfies the nonhomogeneous Schrödinger equation

$$-\frac{1}{2}\epsilon^2 (\partial_{xx} \varphi_E^{int} + \partial_{yy} \varphi_E^{int}) + V_e \varphi_E^{int} = E \varphi_E^{int} - V_w \varphi_E^{ext}, \tag{3.5}$$

with the boundary condition

$$\varphi_E^{int}(x,y) \Big|_{\Gamma_d} = 0, \tag{3.6a}$$

$$\epsilon \partial_x \varphi_E^{int}(a,y) = - \sum_{E > E_m^a} i \sqrt{2(E - E_m^a)} \varphi_{E,m}^{int,a} \chi_m^a(y) + \sum_{E \leq E_m^a} \sqrt{2(E_m^a - E)} \varphi_{E,m}^{int,a} \chi_m^a(y), \tag{3.6b}$$

$$\epsilon \partial_x \varphi_E^{int}(b,y) = \sum_{E > E_m^b} i \sqrt{2(E - E_m^b)} \varphi_{E,m}^{int,b} \chi_m^b(y) - \sum_{E \leq E_m^b} \sqrt{2(E_m^b - E)} \varphi_{E,m}^{int,b} \chi_m^b(y). \tag{3.6c}$$

Then we approximate it by the multi-mode form

$$\varphi_E^{int}(x,y) = \sum_{n=1}^N \frac{\theta_n(E)}{\lambda_n - E} \phi_n(x,y). \tag{3.7}$$

Here $\phi_n(x,y)$ is the non-trivial solution of the eigenvalue problem

$$-\frac{1}{2}\epsilon^2(\partial_{xx}\phi + \partial_{yy}\phi) + V_e\phi = \lambda\phi, \tag{3.8}$$

with the boundary condition

$$\phi(x,y)|_{\Gamma_d} = 0, \tag{3.9a}$$

$$\epsilon\partial_x\phi(a,y) = -\sum_{\text{Re}\lambda > E_m^a} i\sqrt{2(\lambda - E_m^a)}\phi_m^a\chi_m^a(y) + \sum_{\text{Re}\lambda \leq E_m^a} i\sqrt{2(E_m^a - \lambda)}\phi_m^a\chi_m^a(y), \tag{3.9b}$$

$$\epsilon\partial_x\phi(b,y) = \sum_{\text{Re}\lambda > E_m^b} i\sqrt{2(\lambda - E_m^b)}\phi_m^b\chi_m^b(y) - \sum_{\text{Re}\lambda \leq E_m^b} i\sqrt{2(E_m^b - \lambda)}\phi_m^b\chi_m^b(y). \tag{3.9c}$$

Taking (3.7)-(3.9) into (3.5)-(3.6) leads to linear system for the coefficients $\theta_n(E)$:

$$\sum_{n=1}^N \langle \phi_n, \phi_{n'} \rangle \theta_n(E) = -\langle V_w \varphi_E^{ext}, \phi_{n'} \rangle. \tag{3.10}$$

4 Numerical examples

In this section, we give two numerical examples to verify the accuracy of the method. We use central difference approximation to discretize the Schrödinger equation. And the boundary conditions are discretized by second order one sided approximation. The ‘true’ solution of the Schrödinger equation (2.5) and (3.1)-(3.2) is solved using small enough mesh size.

Example 4.1. Consider the 1D Schrödinger equation (2.5) on the computational domain $[0,1]$ with parameters

$$\begin{aligned} a_1 &= 0.1, & a_2 &= 0.27, & b_2 &= 0.73, & b_1 &= 0.9, \\ F &= 2, & c_1 &= 0.33, & d_1 &= 0.47, & c_2 &= 0.53, & d_2 &= 0.67, \\ V_0 &= 2, & V_1 &= 1.45, & \epsilon &= 0.035. \end{aligned}$$

This is a double barrier model. We give the curve of transmission coefficients $T(E)$ in Fig. 3 (top). From the figure, we can see three peaks. They correspond to the fourth to sixth eigenvalues of (2.9), see Fig. 4. We plot the absolute and relative l^2 error of the wave function

$$\begin{aligned} e_a^N(p) &= \left\| \varphi_p(x) - \varphi_p^{ext}(x) - \sum_{n=1}^N \theta_n(p)\phi_n(x) \right\|_{l^2}, \\ e_r^N(p) &= \frac{\left\| \varphi_p(x) - \varphi_p^{ext}(x) - \sum_{n=1}^N \theta_n(p)\phi_n(x) \right\|_{l^2}}{\left\| \varphi_p(x) \right\|_{l^2}}, \end{aligned}$$

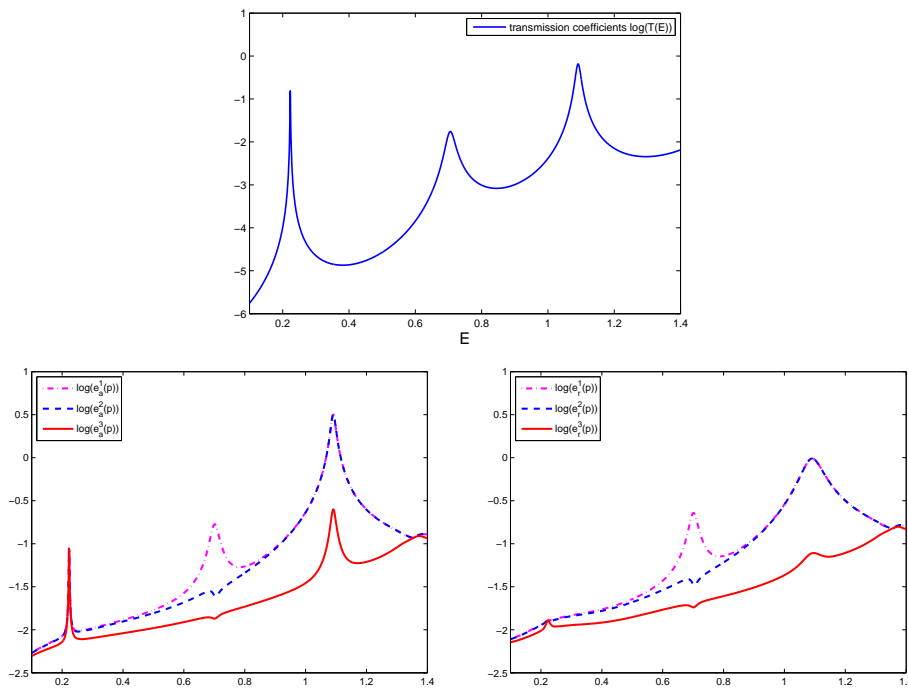


Figure 3: Example 4.1: the top figure is the transmission coefficients $T(E)$, the bottom figures are absolute error $e_a^N(p)$ and relative error $e_r^N(p)$ of wave function for $N=1,2,3$.

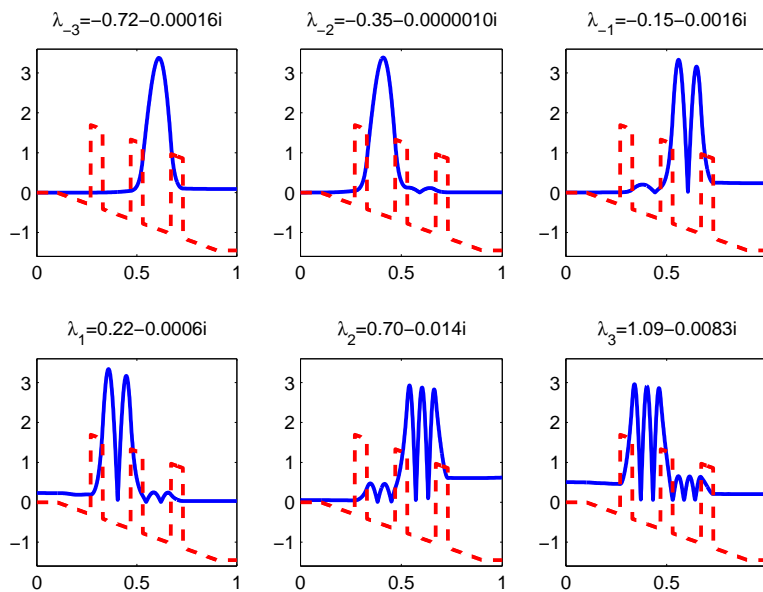


Figure 4: Example 4.1: the first six eigenvalues λ_n and absolute value of eigenfunctions $|\phi_n(x)|$ to the nonlinear eigenvalue problem (2.9).

Table 1: Example 4.1: the relative errors with different space mesh size Δx and energy $E = \frac{1}{2}p^2$ for $N=3$.

	$E=0.2$	$E=0.4$	$E=0.6$	$E=0.8$	$E=1.0$
$\Delta x = \frac{1}{200}$	6.10%	6.99%	9.03%	8.69%	8.52%
$\Delta x = \frac{1}{400}$	3.60%	3.63%	4.39%	4.86%	5.47%
$\Delta x = \frac{1}{800}$	2.04%	1.99%	2.49%	3.07%	4.43%

with different energy $E = \frac{1}{2}p^2$ and number of mode N in Fig. 3 (bottom). Here the space mesh size is fixed as $\Delta x = \frac{1}{800}$. We can see the multi-mode approximation gives more accurate solutions. In Table 1, we output the relative errors with different space mesh size Δx and energy $E = \frac{1}{2}p^2$ for $N=3$. We can see the errors decay with respect to mesh size Δx . The convergence rate is about first order. This can be improved by specially handling the discontinuity of the external potential $V_e(x)$ in the eigenvalue problem (2.9) and make use of a higher order numerical integral in (2.10).

Remark 4.1. Note the real part of first three eigenvalues are negative, but there is almost no interaction with the incoming wave on the left with momentum $p \geq 0$. Therefore, we ignore these eigenvalues in the multi-mode approximation.

Remark 4.2. The convergence rate in Table 1 is not exact first order. The reason is that there are mainly two parts of the error. The first part error comes from the discretization of space which related to Δx . Another part error comes from the decomposition which related to N . Since we fixed $N=3$, the decomposition error would effect or even dominate the total error when the discretization error is small during the space mesh size Δx is reducing.

Example 4.2. Consider the 2D Schrödinger equation (3.1)-(3.2) on the computational domain $\Omega = [0,1] \times [-0.5,0.5]$ with parameters

$$\Omega_b = ([0,1] \times [-0.5, -0.3]) \cup ([0,1] \times [0.3, 0.5]) \cup ([0.2, 0.8] \times [-0.3, 0.3]),$$

$$F = 1, \quad \Omega_1 = [0.4, 0.6] \times [-0.1, 0.1], \quad V_0 = 1, \quad V_1(y) = 0, \quad \epsilon = 0.1.$$

Then we have

$$E_m^a = E_m^b, \quad \chi_m^a(y) = \chi_m^b(y),$$

to the eigenvalue problems (3.3). In Table 2, we output their first eight eigenvalues. From which we can believe that $M=8$ is accurate enough for the boundary conditions (3.2),

Table 2: Example 4.2: the first eight eigenvalues of (3.3).

m	1	2	3	4	5	6	7	8
E_m^a	0.027	0.109	0.245	0.431	0.663	0.925	1.159	1.289

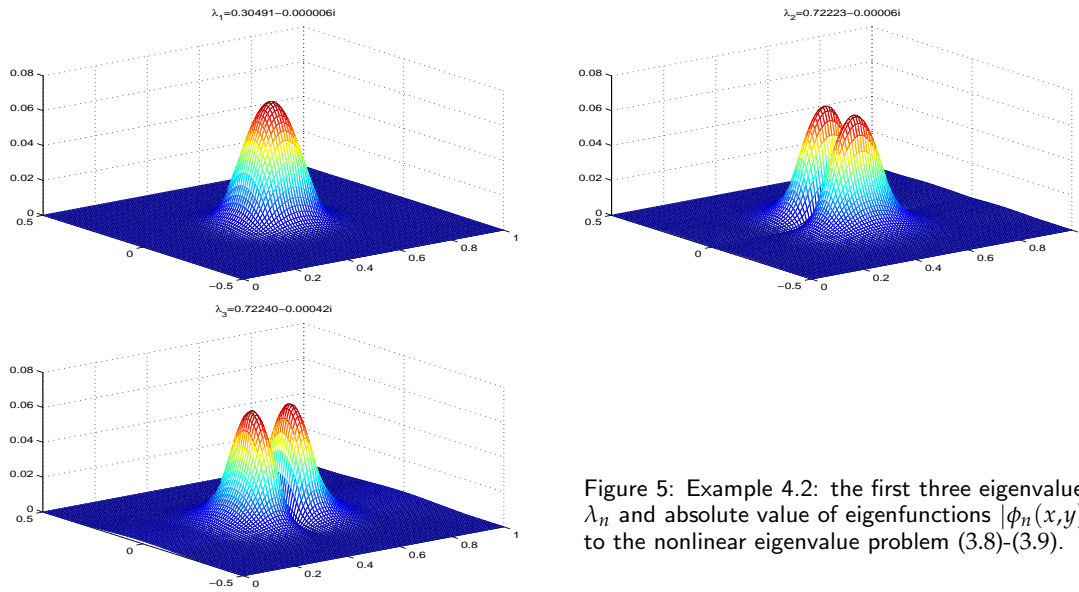


Figure 5: Example 4.2: the first three eigenvalues λ_n and absolute value of eigenfunctions $|\phi_n(x,y)|$ to the nonlinear eigenvalue problem (3.8)-(3.9).

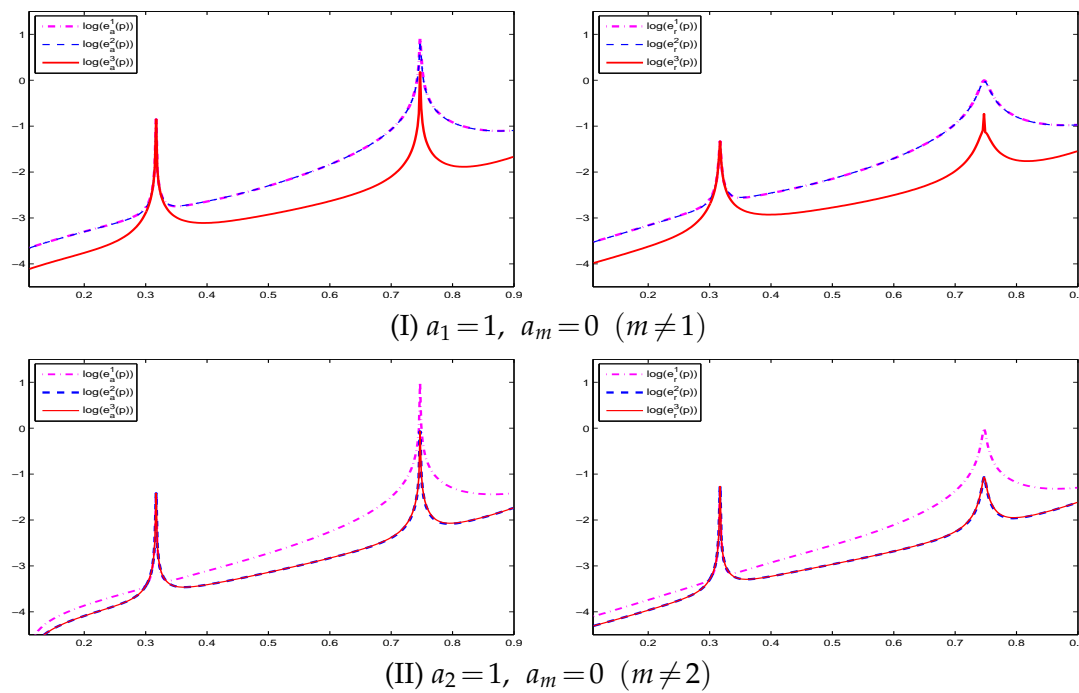


Figure 6: Example 4.2: absolute error $e_a^N(E)$ and relative error $e_r^N(E)$ of wave function for $N=1,2,3$.

(3.6) and (3.9) when $E \leq 1$. We also plot the first three eigenfunctions of (3.8)-(3.9) in Fig. 5, which correspond to the resonance effect. In Fig. 6, we plot the absolute and relative l^2

error of the wave function

$$e_a^N(E) = \left\| \varphi_E(x,y) - \varphi_E^{ext}(x,y) - \sum_{n=1}^N \theta_n(E) \phi_n(x,y) \right\|_{l^2},$$

$$e_r^N(E) = \frac{\left\| \varphi_E(x,y) - \varphi_E^{ext}(x,y) - \sum_{n=1}^N \theta_n(E) \phi_n(x,y) \right\|_{l^2}}{\|\varphi_E(x,y)\|_{l^2}},$$

with different energy E and number of mode N . Here the space mesh size is fixed as $\Delta x = \Delta y = \frac{1}{200}$ and the incoming waves in (3.2) are given by

- (I) $a_1 = 1, a_m = 0 (m \neq 1)$, see Fig. 6 (top),
- (II) $a_2 = 1, a_m = 0 (m \neq 2)$, see Fig. 6 (bottom).

From the figure, we can draw the same conclusion as in Example 4.1.

5 Discussion for algorithm efficiency

In this section, we discuss the algorithm efficiency in computing the electronic density $n(x)$. To compute the integral (2.4) numerically

$$n(x) = \int_{-\infty}^{+\infty} g(p) |\varphi_p(x)|^2 dp,$$

we need to first discretize the energy mesh then compute $\varphi_p(x)$ for each energy mesh point $E = \frac{1}{2}p^2$. Because $\varphi_p(x)$ would be very large near the resonant energy, the energy mesh should resolve these peaks to acquire enough accuracy. There are mainly four methods to compute $n(x)$.

1. The multi-mode approximation.

1. Solve the nonlinear eigenvalue problem (2.9) to get the smallest K_e resonant energies and the related eigenfunctions. The space mesh size is Δx , and the following steps are the same.
2. Compute N_c times nonhomogeneous Schrödinger equation (2.6) to get these exterior wave functions φ_p^{ext} . Here N_c also denote the number of energy nodes for coarse mesh.
3. Interpolate on the energy direction $K_e N_a$ times to get the additional exterior wave functions φ_p^{ext} on a refined energy mesh. Here N_a denotes the number of added energy nodes we need for each single resonant energy.
4. Construct the interior wave functions using equation (2.8) and (2.10). The number of interior wave functions we need to solve is equal to the total number of the energy node on the refined mesh $N_c + K_e N_a$. The space mesh for the interior wave functions φ_p^{int} should be Δx .

2. The nonuniform energy grid method. Assume that we prior know where the resonant energy is, then we can design the best nonuniform energy grid. The number of node on the nonuniform energy grid is $N_c + K_e N_a$. Then we solve $N_c + K_e N_a$ times full Schrödinger equation (2.5) on space mesh Δx to get φ_p . In practical simulation, this method can not be applied unless the resonant energy are prior known.

3. The adaptive mesh on energy grid method. In the beginning, we don't know how to design the nonuniform energy grid. The adaptive mesh method would detect and rebuild the energy mesh. Then, we need to compute no less than $N_c + K_e N_a$ times full Schrödinger equation (2.5) on space mesh Δx to get φ_p .

4. The full method. We directly compute N_f time full Schrödinger equation (2.5) space mesh Δx to get φ_p . Here N_f related to a very fine energy mesh and $N_f \gg N_c, N_f \gg K_e N_a$.

In all these method, we ignore the last step: compute the integral (2.4) to get the electronic density $n(x)$. Because this computational cost is minor compare to other steps. It is easy to see the computational cost of the last three methods are

$$\text{nonuniform grid} < \text{adaptive mesh} < \text{full method}.$$

Our goal is to show that the computational cost satisfies

$$\text{multi-mode approximation} < \text{nonuniform grid} < \text{full method},$$

since the nonuniform is more efficient than the adaptive mesh method in practically simulation. This will be done analytical in Subsection 5.1 and numerically in Subsection 5.2.

5.1 A rough estimate of the computational time

Let $M = \lceil \frac{1}{\Delta x} \rceil$, here $\lceil x \rceil$ gives the nearest integral to real number x . For solving a $M \times M$ linear sparse system, we write the computational cost as $\mathcal{L}(M)$. For conjugate gradient method $\mathcal{L}(M) = P_1 M$, with P_1 related to the numbers of iteration and the averaged element number in each row of the matrix. For a standard interpolation method, we write the computational cost as P_2 , which related to the number of nodes used in the interpolation. Now we estimate the computational cost of the d dimension problem for the multi-mode approximation and the nonuniform energy grid method.

1. The multi-mode approximation. The computational cost of each steps are list here

$$C_{mm,a} \approx K_e K_i \mathcal{L}(M^d),$$

$$C_{mm,b} \approx N_c \mathcal{L}(M^d),$$

$$C_{mm,c} \approx K_e N_a P_2 M^d,$$

$$C_{mm,d} \approx (K_e N_a + N_c) M^d.$$

Here K_i comes from solving the nonlinear eigenvalue (2.9). If we use the Newton-like algorithm, K_i denotes number of the iterations. Therefore the total computational cost is

$$C_{mm} \approx (K_e K_i + N_c) \mathcal{L}(M^d) + (K_e N_a (1 + P_2) + N_c) M^d.$$

2. The nonuniform energy grid method. The total computational cost is

$$C_{ne} \approx (K_e N_a + N_c) \mathcal{L}(M^d).$$

3. The full method. The total computational cost is

$$C_{fm} \approx N_f \mathcal{L}(M^d).$$

In later subsection, we will compare this result with the experiment tests.

5.2 The numerical experiments of the computational time

In this subsection, we give two numerical examples to verify the efficiency of the method. The reference solution is computed on a very small energy mesh and space mesh. We use conjugate gradient method to solve the linear system. The linear interpolation is used here, with $P_2 \approx 10$. And $K_i = 6$ would be good enough to give an accurate iteration solution of the eigenvalue problem (2.9).

Example 5.1. Consider the same condition in Example 4.1, the other parameters are

$$\begin{aligned} d = 1, \quad \Delta x = \frac{1}{1600}, \quad M = 1600, \quad P_1 \approx 280, \\ K_e = 3, \quad N_c = 100, \quad N_a = 50, \quad N_{f,1} = 500, \quad N_{f,2} = 1000, \\ g(p) = \frac{3}{5} \log\left(1 + e^{\frac{10-25p^2}{8}}\right). \end{aligned}$$

In Table 3, we output the estimate computational cost, practical computational time and the relative l^2 error of the electronic density $n(x)$ for different methods. From the table, we can see the multi-mode approximation is more efficient.

Table 3: Example 5.1: comparisons of the multi-mode approximation, nonuniform grid method and the full method.

	estimate cost	CPU time	l^2 error
multi-mode approximation	1.00	48.6s	2.06%
nonuniform grid	2.02	97.7s	2.21%
full method ($N_{f,1} = 500$)	4.02	202.0s	4.12%
full method ($N_{f,2} = 1000$)	8.05	400.7s	1.70%

Example 5.2. Consider the same parameters as in Example 4.2, the other parameters are

$$d=2, \quad \Delta x = \frac{1}{400}, \quad M=400, \quad P_1 \approx 2200,$$

$$K_e=3, \quad N_c=100, \quad N_a=40, \quad N_f=1000,$$

$$g_1(E) = \begin{cases} 0, & E < E_1^a, \\ \frac{3}{5} \log(1 + e^{\frac{5-25E}{4}}), & E \geq E_1^a, \end{cases}$$

$$g_2(E) = \begin{cases} 0, & E < E_2^a, \\ \frac{3}{5} \log(1 + e^{\frac{5-25E}{4}}), & E \geq E_2^a. \end{cases}$$

Then the electronic density are given by

$$n(x,y) = \int_0^{+\infty} \left(\sqrt{\frac{2}{E-E_1^a}} g_1(E) |\varphi_E^1(x,y)|^2 + \sqrt{\frac{2}{E-E_2^a}} g_2(E) |\varphi_E^2(x,y)|^2 \right) dE,$$

here $\varphi_E^s(x)$ ($s=1,2$) is the solution to Eqs. (3.1)-(3.2) with $a_s=1, a_m=0(m \neq s)$. In Table 4, we output the estimate computational cost, practical computational time and the relative l^2 error of the electronic density $n(x,y)$ for different methods. From the table, we can draw the same conclusion as in Example 5.1.

Table 4: Example 5.2: comparisons of the multi-mode approximation, nonuniform grid method and the full method.

	estimate cost	CPU time	l^2 error
multi-mode approximation	1.00	1.9×10^4 s	2.81%
nonuniform grid	1.85	3.7×10^4 s	2.55%
full method	8.43	1.5×10^5 s	2.70%

6 Conclusion

In this paper, we developed the multi-mode approximation to compute the Schrödinger equation, that is the basic mode for the RTD. This kind of approximation can handle multiple barrier problems and high dimensional situations. Several examples are given to demonstrate the accuracy and efficiency of this numerical method.

Acknowledgments

During this research, H. Wu benefited from a Post Doc position supported by the Conseil regional Midi Pyrénées (<http://www.midipyrenees.fr/>) entitled "Méthodes Numériques Multi-échelles pour le transport quantique" and by the ANR Project No. BLAN07-2 212988 entitled "QUATRRAIN"). H. Wu would also acknowledge support from NSFC Projects 11071139 and NSFC Projects 10971115.

References

- [1] N. Ben Abdallah, On a multidimensional Schrödinger-Poisson scattering model for semiconductors, *J. Math. Phys.*, 41(2000), no. 7, 4241-4261.
- [2] N. Ben Abdallah, P. Degond and P.A. Markowich, On a one-dimensional Schrödinger-Poisson scattering model, *Z. angew. Math. Phys.*, 48(1997), 135-155.
- [3] N. Ben Abdallah, C. Negulescu, M. Mouis and E. Polizzi, Simulation Schemes in 2D Nanoscale MOSFETs: A WKB Based Method, *J. Comput. Elect.*, 3(2004), 397-400.
- [4] N. Ben Abdallah and O. Pinaud, Multiscale simulation of transport in an open quantum system: Resonances and WKB interpolation, *J. Comput. Phys.*, 213(2006), no. 1, 288-310.
- [5] W.Z. Bao, S. Jin and P.A. Markowich, On time-splitting spectral approximations for the Schrödinger equation in the semiclassical regime, *J. Comput. Phys.*, 175(2002), 487-524.
- [6] W.Z. Bao, S. Jin and P.A. Markowich, Numerical studies of time-splitting spectral discretizations of nonlinear Schrödinger equations in the semiclassical regime, *SIAM J. Sci. Comput.*, 25(2003), no. 1, 27-64.
- [7] S. Datta, *Electronic Transport in Mesoscopic Systems*, Cambridge University Press, 1995.
- [8] S. Datta, *Quantum Transport: Atom to Transistor*, Cambridge University Press, 2005.
- [9] A. Faraj and N. Ben Abdallah, An improved transient algorithm for resonant tunneling, preprint.
- [10] D.K. Ferry and S.M. Goodnick, *Transport in Nanostructures*, Cambridge University Press, 1997.
- [11] H.K. Gummel, Self-consistent iterative scheme for one-dimensional steady state transistor calculation, *IEEE Trans. Electron Devices*, 11(1964), 455-465.
- [12] H.Y. Jiang, W. Cai and R. Tsu, Accuracy of the Frenley inflow boundary condition for Wigner equations in simulating resonant tunneling diodes, *J. Comput. Phys.*, 230(2011), 2031-2044.
- [13] H.Y. Jiang, S.H. Shao, W. Cai and P.W. Zhang, Boundary treatments in non-equilibrium Green's function(NEGF) methods for quantum transport in nano-MOSFETs, *J. Comput. Phys.*, 227(2008), no. 13, 6553-6573.
- [14] S. Jin, H. Wu and X. Yang, Gaussian beam methods for the Schrödinger equation in the semiclassical regime: Lagrangian and Eulerian formulations, *Commun. Math. Sci.*, 6(2008), no. 4, 995-1020.
- [15] S. Jin, H. Wu and X. Yang, A numerical study of the Gaussian beam method for Schrödinger-Poisson equations, *J. Comput. Math.*, 28(2010), no. 2, 261-272.
- [16] G. Jona-Lasinio, C. Presilla and J. Sjöstrand, On Schrödinger equations with concentrated nonlinearities, *Ann. Phys.*, 240(1995), 1-21.
- [17] C. Lent and D. Kirkner, The quantum transmitting boundary method, *J. Appl. Phys.*, 67(1990), 6353-6359.
- [18] P.A. Markowich, P. Pietra and C. Pohl, Numerical approximation of quadratic observables of Schrödinger-type equations in the semiclassical limit, *Numerische Mathematik*, 81(1999), no. 4, 595-630.
- [19] P.A. Markowich, P. Pietra, C. Pohl and H.P. Stimming, A Wigner-measure analysis of the Dufort-Frankel scheme for the Schrödinger equation, *SIAM J. Numer. Anal.*, 40(2002), no. 4, 1281-1310.
- [20] P.A. Markowich, C. Ringhofer and C. Schmeiser, *Semiconductor Equations*, Springer Verlag Wien, 1990.
- [21] H. Mizuta and T. Tanou, *The Physics and Applications of Resonant Tunneling Diodes*, Cam-

bridge University Press, 1995.

- [22] D. Pathria, J.L.L. Morris, Pseudo-spectral solution of nonlinear Schrödinger equations, *J. Comput. Phys.*, 87(1990), no.1, 108-125.
- [23] O. Pinaud, Transient simulations of a resonant tunneling diode, *J. Appl. Phys.*, 92(2002), no. 4, 1987-1994.
- [24] E. Polizzi and N. Ben Abdallah, Subband decomposition approach for the simulation of quantum electron transport in nanostructures, *J. Comput. Phys.*, 202(2005), no. 1, 150-180.
- [25] C. Presilla and J. Sjöstrand, Transport properties in resonant tunneling heterostructures, *J. Math. Phys.*, 37(1996), no. 10, 4816-4844.
- [26] S.H. Shao, W. Cai and H.Z. Tang, Accurate calculation of Green's function of the Schrödinger equation in a block layered potential, *J. Comput. Phys.*, 219(2006), no. 2, 733-748.
- [27] C. Weisbuch and B. Vinter, *Quantum Semiconductor Structures: Fundamentals and Applications*, Academic Press, 1991.